International Journal of Modern Manufacturing Technologies
ISSN 2067–3604, Vol. XIV, No. 1 / 2022
https://doi.org/10.54684/ijmmt.2022.14.1.14

NUMERICAL INVESTIGATION OF CUTTING STABILITY AND SURFACE ROUGHNESS IN ORTHOGONAL MILLING

Wael Baklouti, Charfeddine Mrad, Rachid Nasri

Laboratory of Applied Mechanics and Engineering (LMAI), National Engineering School of Tunis (ENIT), University of Tunis el Manar (UTM), BP 37, Le Belvedere 1002, Tunis, Tunisia.

Corresponding author: Wael Baklouti, waelbaklouti@gmail.com

Abstract: The vibrations produced by the chatter phenomenon are harmful for productivity in material removal machining. Some of the intolerable effects are: workpiece poor surface quality, tool wear, machine lifetime reduction. The flexibility of the cutting system favors vibrations especially when the cutting conditions are inconvenient. The flexibility is mainly linked to the cutting tool, which explains the consideration of the cutting tool as flexible in most of the analytical and numerical literature works. This work presents a numerical approach to investigate the orthogonal metal milling in order to study the chatter phenomenon effect on cutting stability and surface roughness. The proposed approach for numerical simulation uses the ABAQUS software, and includes a flexible tool on the immersion direction as well as on the feed direction. An explicit scheme and a Lagrangian formulation are retained, and the Johnson-Cook laws of behavior and damage are considered. The validation of the numerical results is conducted using experimental results.

Key words: Orthogonal Milling; Chatter Vibration; Numerical Investigation; Cutting Stability; Surface Roughness.

1. INTRODUCTION

Material removal machining at high cutting speeds and large cutting depths produces workpieces with poor surface quality and causes damage to the cutting system. This is due to the appearance of chatter vibrations, which influence the planned path of the tool during machining. The occurrence of vibrations depends mainly on the dynamic behavior of machine-tools. The instability of the cutting system introduces the variation of the chip section, therefore variation of the cutting forces. The instability of the cutting system manifests by poor quality of the machined surface and by excessive noise. The first scientific study of this phenomenon was elaborated by Taylor in 1907 [1], then we may quote Arnold in 1946 [2], Tlusty and Polatek in 1963 [3], and Tobias in 1965 [4]. Merrit in 1965 [5] started the notion of the analytical and experimental stability lobes in orthogonal cutting, consequently the construction of stability lobes became one of the methods followed for the prevention from chatter vibration in machining. This contributed to the conduction of other works, we mention for example: Atintas in 2000 [6], and Erol Turkes et al. in 2012 [7]. Following computer technology evolution, numerical simulation becomes one of the methods used for the construction of stability lobes. Several works were elaborated in this context, as Elbestawi et al. [8], and Ahmadi and Ismail [9]. Other works are carried out using software with a graphical interface, where several important cutting details can appear such as: chip morphology, machined surface, and vibrations of the cutting tool. We note also the work of Mahnama and Movahhedy in 2010 [10], the authors used the software MC-MARC, and the work of Baklouti et al. in 2018 [11], where the authors used the software ABAQUS, to construct stability lobes in orthogonal metal turning. The acute vibrations during machining lead the cutting tool outside the manufacturer planned path. The new tool trajectory defines the shape of the machined surface. Wojciechowski et al. [12], and Wojciechowski and Krzysztof [13] found that the instantaneous movement and deflection of the tool are the main cause that defines the shape of the machined surface.

The current work presents a numerical approach to investigate orthogonal metal milling, the milling process is half-immersion up-milling. The cutting stability and the surface roughness are studied. Experimental results from literature are used to validate the approach.

2. MACHINING STABILITY

According to the stability diagram, stable machining can be carried out by choosing the combinations (speed and depth of cut) of cutting in the stable zone or in the zone of process damping. Figure 1 shows the different regions of a stability diagram. The lobe is the curve obtained in terms of cut depths as function of rotation speeds. The upper part of the diagram, limited by the lobe, represents the unstable zone and the lower part of the diagram represents the stable zone. The adjacent zone simultaneously to the stable zone and to the unstable zone is the process damping zone. It is the zone of low speeds, where the damping of the cutting system ensures the cutting stability.

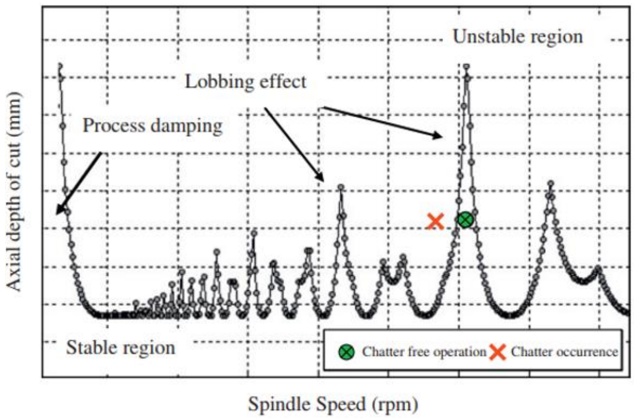

Fig. 1. A stability diagram [14]

3. EXPERIMENTAL RESULTS

The experimental tests carried out by Ahmadi and Ismail [9] are taken as reference for this work. The experimental study was used by the authors to validate a numerical stability lobe established using the semi-discretization method for the milling process in half-immersion up-milling (Figure 2).

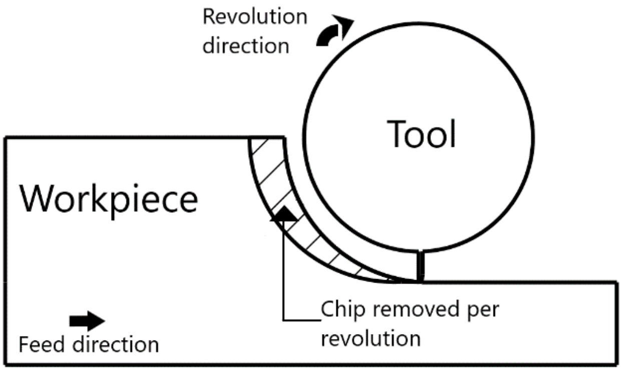

Fig. 2. Milling process in half-immersion up-milling

The used tool is a *25.4mm* diameter end mill, with a single carbide tooth with a clearance angle equal to *7°* and a flank wear width of *0.08mm*. The tool suspension parameters along the x-axis (feed direction) and the y-axis (radial direction): stiffness, damping, natural frequency, and damping rate, are respectively: $k_x=4.74N/\mu m$ and $k_y=4.27N/\mu m$, $c_x=65.30Ns/m$ and $c_y=60.78Ns/m$, $f_x=346Hz$ and $f_y=336Hz$, $\zeta_x=0.015$ and $\zeta y=0.015$. The tests on the alloy 7075T6 were made using DCKEL-MAHO 5-axis milling center.
The friction between the workpiece and the tool is characterized by the Coulomb coefficient $\mu=0.3$. The feed rate per tooth for all tests is equal to *St=0.05mm/tooth*. Measurements have led to two cutting forces, divided by the depth of cut in the radial direction.

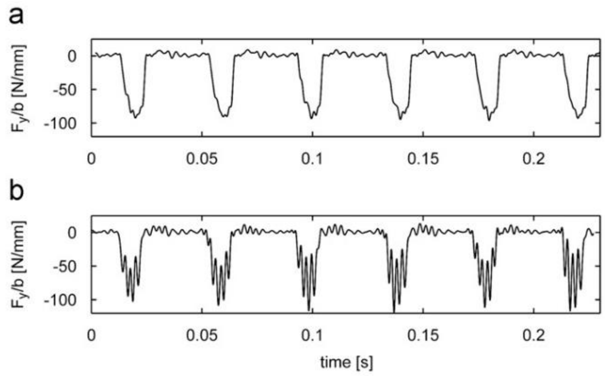

Fig. 3. Experimental cutting forces for N=1500rpm: (a) ap=1mm, (b) ap=1.5mm [9]

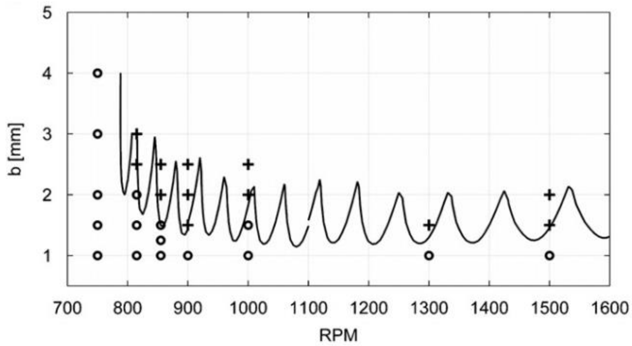

Fig. 4. Experimental stability diagram (b=ap) [9].

Figure 3 shows the cutting force for the rotational speed *N=1500rpm* and the cut depths respectively *ap=1mm* and *ap=1.5mm*. (a) shows the force in the case of a stable cut (without chatter), the cutting force in this case admits small fluctuations and keeps maximum absolute values F_{max} approximately *100N/mm*. (b) shows the force in the case of unstable cutting (with chatter) which can be distinguished by large fluctuations and maximum absolute values F_{max} exceeds *120N/mm*. These measurements are made using a table dynamometer, Kistler 9255. A numerical stability lobe was established using the semi-discretization method (curve in black) and the experimental tests (circles for stable tests and crosses for unstable tests) are noted, Figure 4.

4. NUMERICAL MODELING

The ABAQUS software is considered. A Lagrangian formulation [15, 16] is adopted for the numerical tests. This formulation guarantees, compared to the Eulerian formulation and to the Lagrangian-Eulerian formulation, a machined surface, a chip morphology and a cutting force, closer to reality. We note in this context, works where the Lagrangian formulation is confirmed for the numerical simulation of machining, Mahnama and Movahhedy [10] and Baklouti et al. [11]. The explicit scheme is adopted for this study following its convergence for large deformations, unlike the implicit scheme which presents difficulties of convergence for the treated problem [17]. The simulations are made for a single pass. The law of Coulomb, defined by equation (1), designates the contact between the workpiece and the tool.

$$\tau_{cri}=\mu_0 \times p \quad (1)$$

μ_0,p, and τ_{cri}, represent respectively the coefficient of friction, the pressure between the two contact surfaces, and the critical shear stress.

The meshing of the tool and of the workpiece is made using numerical measurements based on the experimental results.

The simulation is done firstly without introducing the thermal effect, the CPE4R (generalized plane strain mesh element, 4-node bilinear, reduced integration with hourglass control) element is used for the first model.

The simulation is done secondly with introducing the thermal effect in order to determine its influence on the stability of the cut. The CPE4RT (coupled temperature-displacement plane strain mesh element, 4-node bilinear displacement and temperature, reduced integration with hourglass control) element is used for the second model.

4.1. Tool details

The cutting tool considered for numerical simulation is modeled as a linear dynamic system (mass, spring, damper) with two degrees of freedom, and of two directions: immersion and feed. The suspension parameters and the dimensions used for the experimental tests are adopted for the numerical tests. The tool is considered rigid, which makes any possible deformation within the springs and the dampers. The tool admits a single rotational movement along the z-axis. The mesh elements of the tool in the cutting area are of dimension: *4µm* in width and *3.5µm* in height. All the tool details are mentioned in Figure 5.

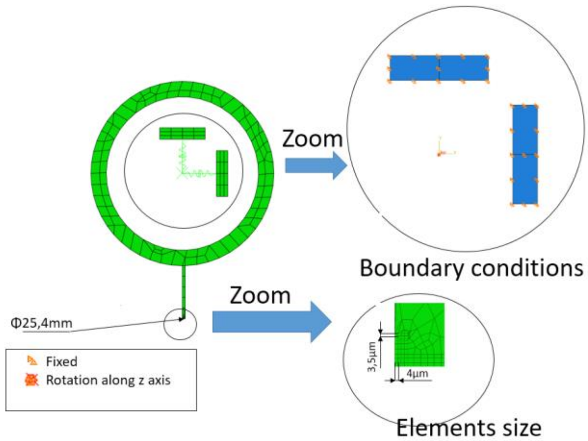

Fig. 5. Tool modeling

4.2 Workpiece details

The workpiece used for the numerical simulation has a quarter circle form, as shown in Figure 6. The dimensions of the mesh elements in the cutting area are: *40µm* in width and *9µm* in height. The workpiece is fixed along the y-axis and the feed speed is along the x-axis. The Johnson-Cook model is taken for material behavior, it is defined by equation (2), Where *A* is the yield strength, *B* is the strain hardening modulus, and n is the strain-hardening coefficient. *C* corresponds to the coefficient of dependence on the strain-hardening speed. ε, $\dot{\varepsilon}$ are respectively the shear strain, the shear strain velocity. The coefficient *m* represents the heat-softening exponent. The ambient, transition, and melting temperatures of the material are respectively, θ, θ_t, θ_m.

Table 1. Alloy 7075T6 physical and mechanical proprieties [20, 21]

Physical and mechanical properties		
Physical	E (MPA)	71700
	ρ (kg/m^3)	2800
	ν	0.33
Mechanical	k_{ic} (MPa.m$^{1/2}$)	28
	σ_y (Mpa)	565

Table 2. Alloy 7075T6 Johnson-Cook parameters [19]

Johnson-Cook parameters		
Strength Constants	*A(MPa)*	546
	B(MPa)	678
	C	0.024
	n	0.71
	m	1.56
	θ_t (°C)	477
	θ_m (°C)	30
Fracture Constants	D1	-0.068
	D2	0.451
	D3	-0.952
	D4	0.036
	D5	0.697

$$\sigma = [A + B\varepsilon^n] \times \left[1 + C \ \ln\frac{\dot{\varepsilon}}{\dot{\varepsilon}_0}\right] \times \left[1 - \left(\frac{\theta - \theta_t}{\theta_m - \theta_t}\right)^m\right] \quad (2)$$

The Johnson-Cook model is also taken for material damage, it is defined by equation (3).

$$\varepsilon_f = [D_1 + D_2 exp(-D_3\eta)] \times \left[1 + D_4 \ \ln\frac{\dot{\varepsilon}}{\dot{\varepsilon}_0}\right] \times \left[1 - D_5\left(\frac{\theta - \theta_t}{\theta_{melting} - \theta_t}\right)^m\right] \quad (3)$$

With D_1, D_2, D_3, D_4, and D_5 are the fracture constants of Johnson-Cook. According to ABAQUS Manuel [18], it is necessary to define a displacement or an energy, which are defined respectively by equations (4) and (5), for the initiation to the fracture.

$$u_f = \frac{2G_f}{\sigma_y} \tag{4}$$

$$G_f = \left(\frac{1-\nu^2}{E}\right) \times k_{ic}^{\ 2} \tag{5}$$

With k_{ic}, G_f, σ_y, ν and E are respectively the fracture toughness, the fracture energy, the yield stress, the Poisson Ratio, and the Young modulus. Tables 1 and 2 respectively show the parameters of the alloy 7075T6 and the associated Johnson-Cook constants. The strain rate considered for the simulation is $\dot{\varepsilon}=10^{-3}$. The calculation led to u_f=*38µm*.

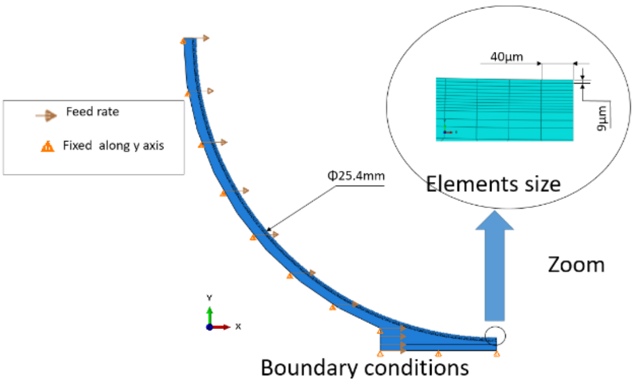

Fig. 6. Workpiece modeling

4.3 Cutting details

The simulation is made for a 2D half-immersion up-milling machining. Only one pass is simulated for each combination of cutting speed and cut depth. For up-milling process, theoretically the chip section for each pass evolves from *zero* to a maximum value envisaged by the manufacturer. In practice, the chip section begins to occur from a minimum chip value associated with the tool. The usual values of the minimum chip in milling for a carbide tool are between *0.03mm* and *0.05mm*. Numerical tests for minimum chip values of *0.03mm*, *0.04mm*, and *0.05mm*, led to mismatched cutting force values. The closest values compared to the experimental values are those found by admitting a minimum chip equal to *0.03mm*, therefore this value is retained. The Cutting details and the minimum chip setting are shown in Figure 7.

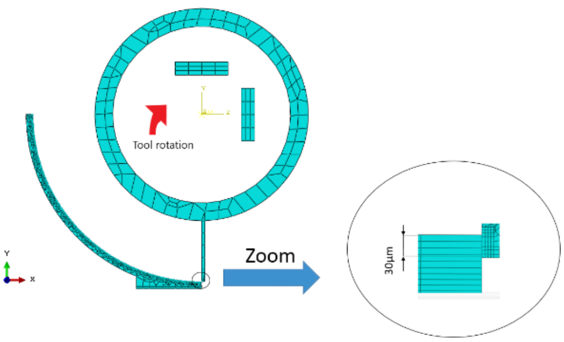

Fig. 7. Material cutting: minimum chip setting

The same combinations of cutting speeds and depths of cut used for the experimental tests are used for the numerical tests.

5. NUMERICAL RESULTS

The cutting stability and the surface roughness are examined using the cutting forces then the tool accelerations, since they lead to different stability results.

5.1 Simulation without thermal effect

5.1.1 Using the cutting forces

Three states of cutting stability can arise in machining by material removal, stable cutting state, cutting state at the limit of stability (considered as stable) and unstable cutting state. Numerical simulations started with a speed of *N=1500rpm* in order to determine the three states of stability, using the cutting forces and the surface finish. Following the numerical results as varying the depth of cut for the speed *N=1500rpm*, three states of stability are found, for *ap=1mm* (stable cut), for *ap=1.23mm* (cut at the limit of stability), and for *ap=1.5mm* (unstable cut). Figure 8 represents the cutting forces along the y-axis divided by the associated depth of cut for *ap=1mm*, *ap=1.23mm*, and *ap=1.5mm*. Figure 9 shows the surface finish for the three tests.

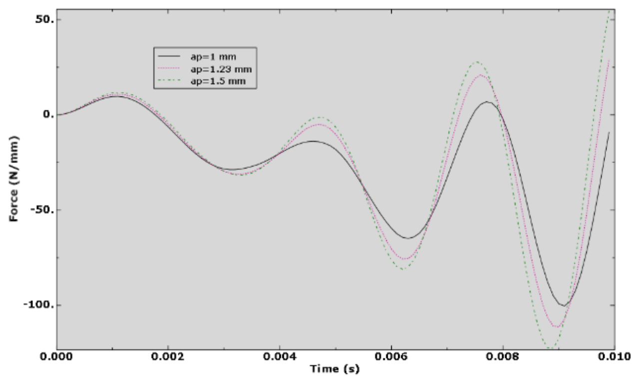

Fig. 8. Cutting forces for N=1500rpm: ap=1mm (stable), ap=1.23mm (stability limit), ap=1.5mm (unstable)

We note that the forces found numerically in the case of stable cut (*N=1500rpm*, *ap=1mm*; $F_{max}\approx 100N/mm$) and in the case of unstable cut (*N=1500rpm*, *ap=1.5mm*; $F_{max}>100N/mm$), have maximum absolute values in agreement with the maximum absolute values found experimentally. Furthermore, examining the forces pace, the fluctuation of the cutting force in the case of unstable cutting is greater than in the case of stable cutting, which is in agreement with the experimental results.

Concerning the cutting case in the stability limit (*N=1500rpm*, *ap=1.23mm*) the cutting force has intermediate maximum absolute value and fluctuation.

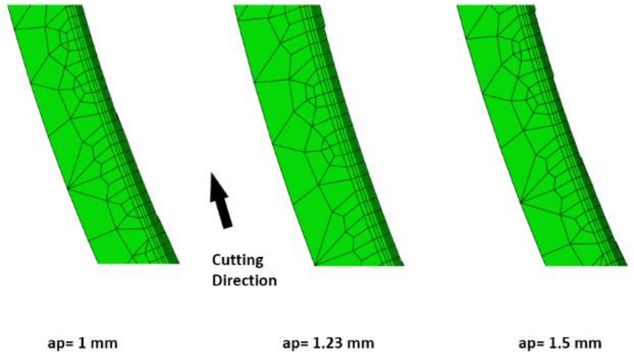

Fig. 9. Surface finish for the three states of stability: ap=1mm (stable), ap=1.23mm (stability limit), ap=1.5mm (unstable)

Regarding the surface quality observed, Figure 9 shows a machined surface portion for each depth of cut. For *ap=1mm*, the machined surface looks to be produced by a stable cut in up-milling, since in such a case the chip evolves from minimum to maximum, therefore the removed section increases continuously over time, then it is a case of stable cutting. For *ap = 1.5mm*, the surface evolution does not keep a continuous increase which reflects the disturbance at the level of the instantaneous displacements of the cutting tool generated by vibrations, therefore it is a case of unstable cutting. For *ap=1.23mm*, the produced surface keeps a continuous evolution but with some disturbances, it is the case of cutting at the limit of stability. These results come to support the results of the cutting forces. The forces found for the speed *N=1500rpm* are taken as reference for the stability classification for the rest of the combinations of tool rotation speed and depth of cut. The simulations led to the establishment of a numerical stability lobe, based on cutting forces, mentioned with a broken line, in Figure 10.

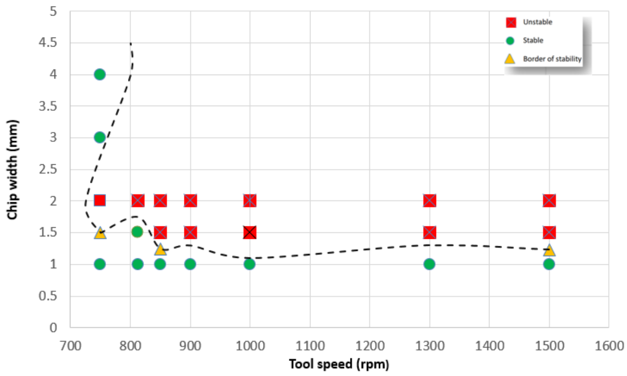

Fig. 10. Numerical stability diagram using cutting forces

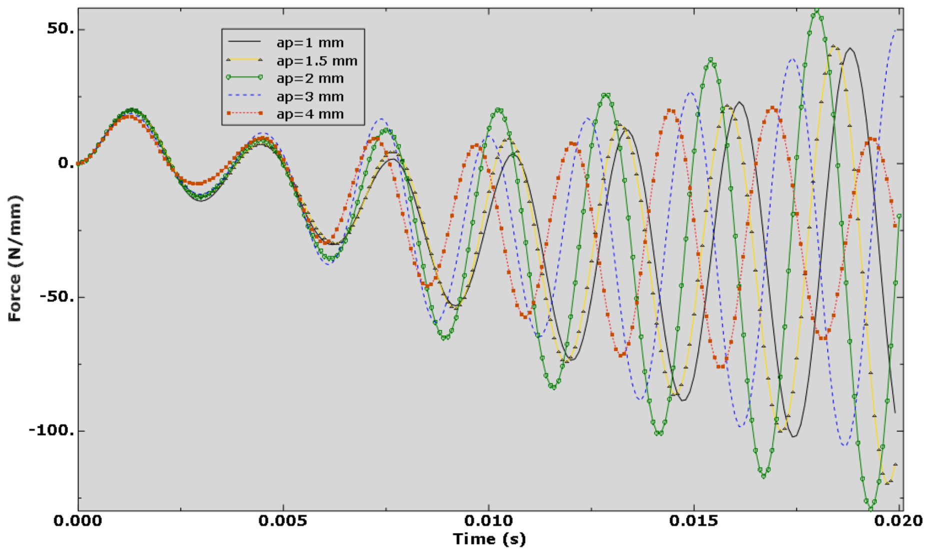

Fig. 11. Cutting forces for N=750rpm

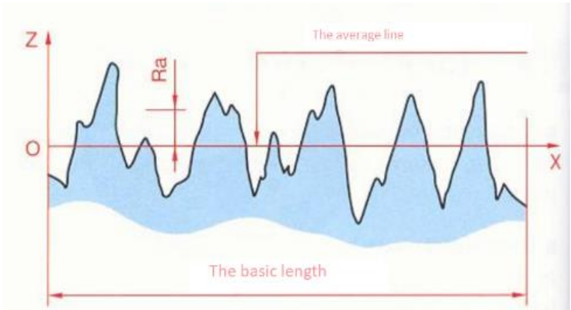

Fig. 12. Arithmetic average roughness definition

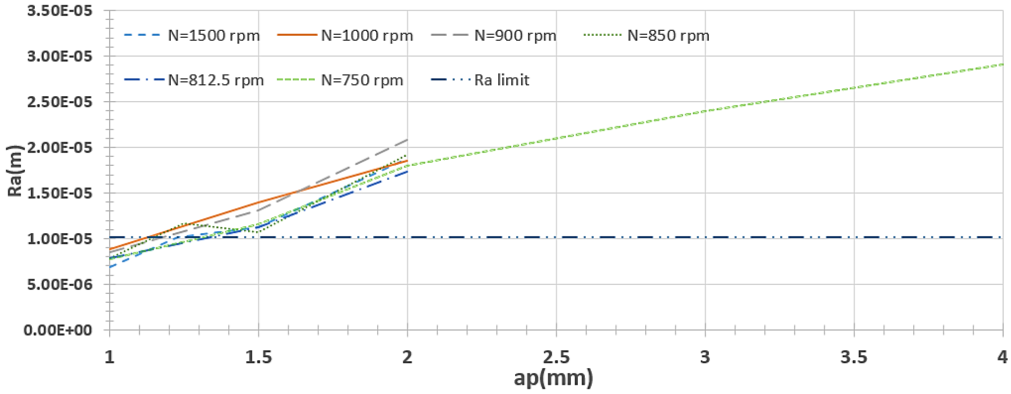

Fig. 13. Arithmetic average roughness evolution

The circles, the triangles, and the squares respectively represent the numerical tests for a stable cut, a cut at the limit of stability, and an unstable cut, respectively.
The obtained, cutting forces-based numerical stability lobe is in agreement with the experimental stability lobe (Figure 4).
For the low speed part (in the vicinity of damping process zone), in particular at the level of N=750rpm, Figure 11 is obtained. Based on the cutting forces, we notice that the cutting stability fluctuates from stable to unstable to stable, in contrast with the high speed part.

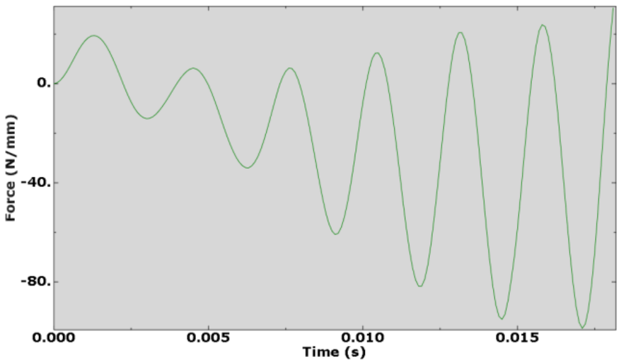

Fig. 14. Cutting force for N=812.5rpm and ap=1.5mm

Now, a surface roughness study is conducted in order to quantify the effect of the chatter vibration on the workpiece surface quality. We use, the arithmetic average roughness criterion *Ra* (Figure 12), defined as shows equation (6).

$$R_a = \frac{|z_1| + \cdots + |z_n|}{n} \tag{6}$$

The method adopted to establish the *Ra* values for each machined surface consists of:
First, we seek the profile of the machined surface using the instantaneous movement dx_i and dy_i respectively in the immersion and the feed directions of the cutting tool. The instantaneous curvature C_i of the profile for each combination dx_i and dy_i is defined by equation (7).

$$C_i = \sqrt{{d_{x_i}}^2 + {d_{y_i}}^2} \tag{7}$$

Second, we seek the average line using the least square method applied to Z_i, which represents the distances of *n* profile points relatively to the average line.
Third, we apply equation (6) to obtain the values of *Ra*. The obtained *Ra* values are presented in Figure 13. The basic length L_b is taken as follows.

$$L_b = \pi \times {}^{r}/_{2}$$
$$L_b = \pi \times {}^{12.7}/_{2} = 19.94mm \tag{8}$$

With *r* is the radius of the machined surface.
Referring to the tests, it is found that *Ra=6.87µm* for a stable cut (case of *N=1500rpm* and *ap=1mm*), *Ra=10.11µm* for a limit of stability cut (case of *N=1500rpm* and *ap=1.23mm*), and *Ra=11.20µm* for an unstable cut (case of *N=1500rpm* and *ap=1.5mm*), to conclude that the surface qualities are in agreement with the cutting forces.
For the speeds *N=1300*, *1000*, *900*, and *850rpm*, there is an agreement between the states of stability using cutting forces and surface quality, unlike the speeds *N=812.5* and *750rpm* where we found a disagreement between the states of stability, for some cut depths (*N=812.5rpm* and *ap=1.5mm*; *N=750rpm* and *ap=1.5*, *3*, *4mm*), around the process damping zone. The cutting force for *N=812.5rpm* and *ap=1*.5mm is shown in Figure 14.

5.1.2 Using the tool accelerations

Three acceleration stages are found for the tests. Figure 15, Figure 16, and Figure 17 respectively show the accelerations along the two directions of study for a stable cut (case of *N=1500rpm* and *ap=1mm*), for a limit of stability cut (case of *N=1500rpm* and *ap=1.23mm*), and for an unstable cut (case of *N=1500rpm* and *ap=1.5mm*).

Accelerations along the x-axis (Ax) are shown in broken line and accelerations along the y-axis (Ay) are presented in continuous line. The accelerations of the stable cut have absolute values of approximately *100m/s²*, while unstable cut accelerations have maximum absolute values exceeding *170m/s²*. For accelerations at the limit of stability, the maximum absolute values are between *100m/s²* and *170m/s²*.

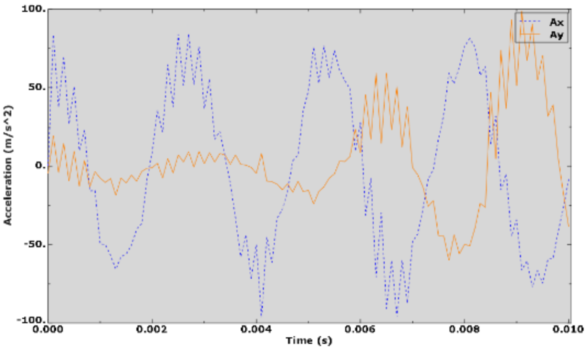

Fig. 15. Accelerations for N=1500rpm and ap=1mm

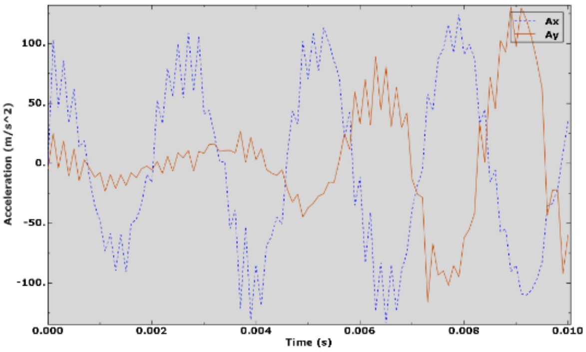

Fig. 16. Accelerations for N=1500rpm and ap=1.23mm

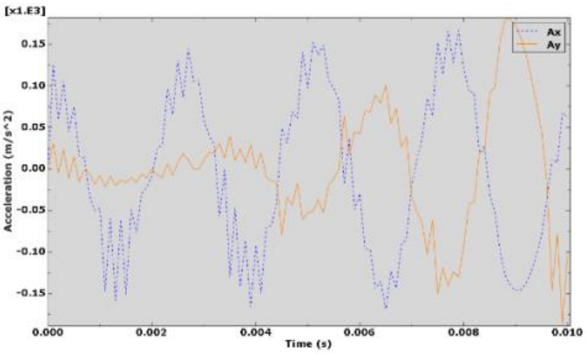

Fig.17. Accelerations for N=1500rpm and ap=1.5mm

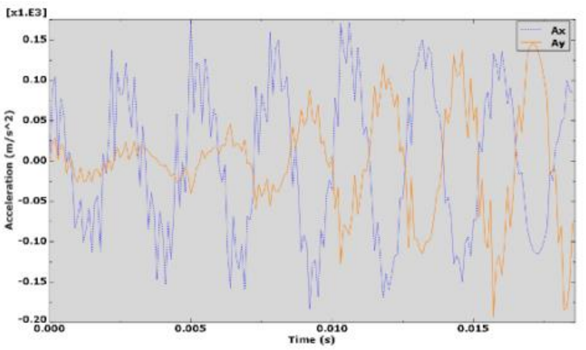

Fig. 18. Accelerations for N=812.5rpm and ap=1.5mm

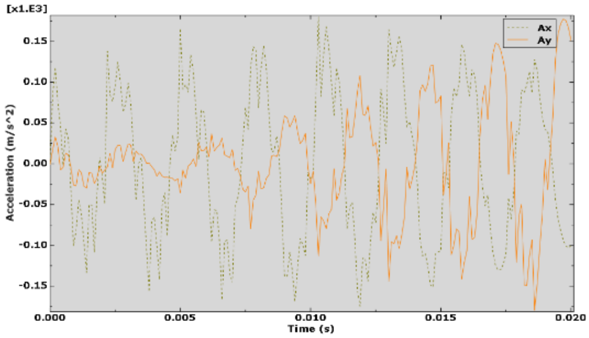

Fig. 19. Accelerations for N=750rpm and ap=1.5mm

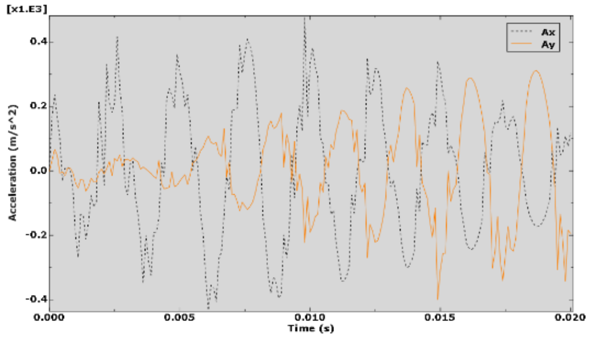

Fig. 20. Accelerations for N=750rpm and ap=3mm

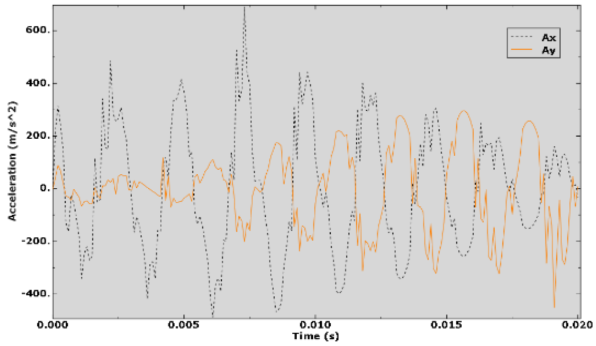

Fig. 21. Accelerations for N=750rpm and ap=4mm

The stability study based on tool accelerations shows agreement with the obtained *Ra* values, but some disagreement with the cutting forces stability. The disagreement is in the process damping zone, case of *N=812.5rpm* and *ap=1.5mm*; and case of *N=750rpm* and *ap=1.5, 3, 4mm*. The accelerations associated to these combinations are shown respectively in Figure 18, Figure 19, Figure 20, and Figure 21.

A stability lobe based on tool accelerations is established, it is presented in Figure 22.

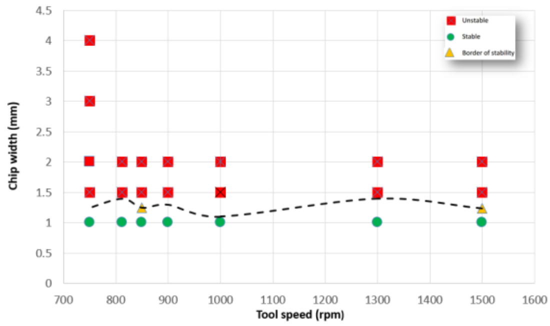

Fig. 22. Numerical stability diagram using tool accelerations

The obtained tool accelerations-based numerical stability lobe is less in agreement with the experimental stability lobe (Figure 4).

5.2 Simulation with thermal effect

The results found without thermal effect led us to consider strengthening the modeling to seek better concordance between the stability based on the cutting forces and the stability based on the tool accelerations in one hand, and with the experimental results in another hand. For this, we introduced the thermal effect in order to take into account the thermomechanical coupling.

Based on the previous tests of the cutting forces shown in Figure 7, and of the tool accelerations shown in Figures 15, 16, and 17, associated to the different states of stability, two stability lobes are found with introducing the thermal effect.

The new stability lobes are not too different from the previous stability lobes, for all the speeds of rotation except for the process damping zone (around *750rpm*) as shows Figure 23. However, the results with thermal coupling are closer to the experimental results (green circles for stable tests and red squares for unstable tests).

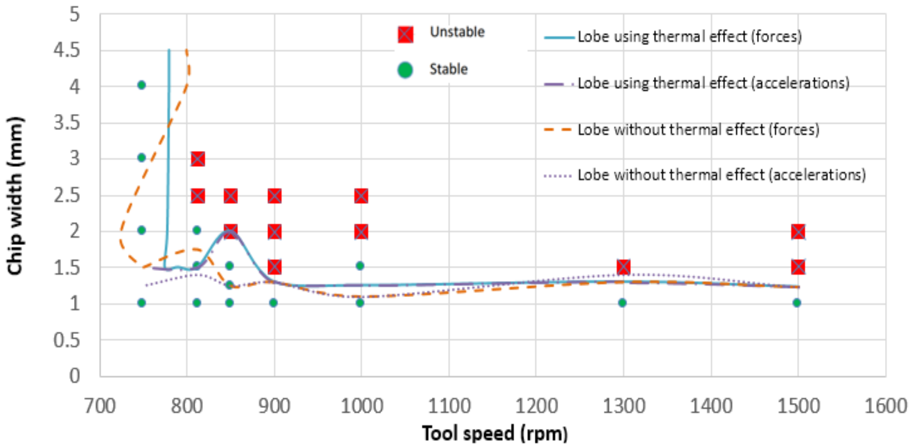

Fig 23. Numerical stability diagrams, with and without thermal effect, in addition to the experimental tests

6. CONCLUSION

This work presented a numerical approach to investigate orthogonal metal milling, the milling process is half-immersion up-milling. The cutting stability and the surface roughness are studied. Experimental results from literature are used to validate the approach.

The approach uses the ABAQUS software, and adopts a flexible tool on the immersion direction as well as on the feed direction. An explicit scheme and a Lagrangian formulation are retained, and the Johnson-Cook laws of behavior and damage are considered. The simulations were done with and without taking into account the thermal effect.

Without thermal effect, the following may be concluded:

•The obtained numerical cutting forces-based stability lobe is in agreement with the experimental stability tests, the only difference is around the process damping zone where a slight instability was observed.

•The obtained numerical tool accelerations-based stability lobe is less in agreement with the experimental stability tests, the difference is also in the process damping zone where a notable instability was observed.

•The tool accelerations method is therefore less accurate then the cutting forces method.

•The obtained machined surface topography, and the determined arithmetic average roughness values describing the machined surface quality, can also predict the cutting instability, but not around the process damping zone.

With thermal effect, the following may be concluded:

•Taking into consideration the thermal effect, the obtained cutting stability lobes basing on the cutting forces and on the tool accelerations are closer to the experimental stability lobe.

•The tool accelerations-based results are in agreement with the experimental results, except in the process damping zone. Whereas, the cutting forces-based results are in agreement with the experimental results, including in the process damping zone.

•The thermomechanical coupling is therefore to be taken into consideration for better prediction accuracy of the cutting stability.

The proposed approach, with thermal effect and basing on the cutting forces, was found capable of predicting accurately the cutting stability in half-immersion up-milling. Furthermore, it is also possible to predict the machined surface quality.

As future works, the damping process zone is to be further studied to align the tool accelerations-based results with the cutting forces-based results.

7. REFERENCES

1. Taylor, F. (1907). *On the art of cutting metals*, Transactions of ASME 28.

2. Arnold, R.N. (1946), *The mechanism of tool vibration in the cutting of steel*, Proceedings of Institution of Mechanical Engineers, pp. 154.

3. Tlusty, J., Polacek, M. (1963), *The stability of machine tools against self excited vibrations in machining*, in: Proceedings of the International Research in Production Engineering Conference, Pittsburgh, PA, ASME, New York, pp. 465–474.

4. Tobias, S.A (1965), *Machine Tool Vibration*, Blackie and Sons Ltd, Glasglow.

5. Merritt, H. E. (1965), *Theory of self-exited machine tool chatter: contribution to machine tool chatter*, Transactions of the ASME Journal of Engineering for Industry, Vol. 87, 447–454.

6. Altintas, Y. (2000), *Manufacturing Automation: Metal Cutting Mechanics*, Machine Tool Vibrations, and CNC Design, Cambridge University press, 286 pages.

7. Turkes Erol, Orak Sezan, Neseli Suleyman, Yaldiz Suleyman (2012), *Decomposition of process damping ratios and verification of process damping model for chatter vibration*, Measurement 45, 1380–1386.

8. Elbestawi, M. A., Ismail, F., Du, R., Ullagaddi, B. C. (1994), *Modelling Machining Dynamics Including Damping in the Tool Workpiece Interface*, Journal of Engineering for Industry ASME, November, Vol. 116/435.

9. Ahmadi, K., Ismail, F. (2012), *Stability lobes in milling including process damping and utilizing Multi-Frequency and Semi-Discretization Methods*, International Journal of Machine Tools & Manufacture 54–55 (2012) 46–54.

10.Mahnama, M., Movahhedy, M.R (2010), *Prediction of machining chatter based on FEM simulation of chip formation under dynamic conditions*, International Journal of Machine Tools & Manufacture 50, 611–620.

11.Baklouti, W., Mrad, C., Nasri, R. (2018), *Numerical study of the chatter phenomenon in orthogonal turning*, Advanced Manufacturing Technology, Vol. 99, No. 1-4, pp. 755-764.

12.Wojciechowski, S., Wiackiewicz, M., Krolczyk, G.M. (2018), *Study on metrological relations between instant tool displacements and surface roughness during precise ball end milling*. Measurement: Journal of the International Measurement Confederation 129, pp. 686-694.

13.Wojciechowski Szymon, Mrozek Krzysztof (2017) *Mechanical and technological aspects of micro ball end milling with various tool inclinations*. International Journal of Mechanical Sciences, 134, pp. 424-435.

14.Quintana Guillem, Ciurana Joaquim (2011), *Chatter in machining processes: A review*, International Journal of Machine Tools & Manufacture 51 363–376.

15.Joyot, P., Rakotomalala, R., Touratier, M. (1993), *Modélisation de l'usinage formulée en Euler-Lagrange Arbitraire*, Journal De Physique iv Colloque C7, supplément au Journal de Physique III, Vol.3, 1141-1144.

16.Schermann, T., Marsolek, J., Schmidt, C., Fleischer J (2006), *Aspects of the Simulation of a Cutting Process with ABAQUS/Explicit Including the Interaction between the Cutting Process and the Dynamic Behaviour of the Machine Tool*. Proceedings of the 9th CIRP International Workshop on Modeling of Machining Operations, Bled, Slovenia, 163–170.

17.Rebelo, N., Nagtegaal, J.C, Taylor, L.M (1992), *Comparison of implicit and explicit finite element and the simulation of metal forming processes"*, Proceedings of the Fourth International Conference on Numerical Methods in Industrial Forming Processes, 1992, pp. 99-108.

18.H.K.S (2013), *Damage initiation for ductile metals, Section 24.2.2 of the ABAQUS Analysis User's Guide*, Version 6.16.

19.Thuc, P., Vo, Z.W., Guan, W.J., Cantwell Schleyer, G.K. (2013), *Modelling of the low-impulse blast behaviour of fibre–metal laminates based on different aluminium alloys*, Composites: Part B 44 (2013) 141–151.

20.Benedetti, M., Fontanari, V., Scardi, P., Ricardo, C.L.A., Bandini, M. (2009), Reverse *bending fatigue of shot peened 7075-T651 aluminium alloy: The role of residual stress relaxation, of residual stress relaxation*, International Journal of Fatigue 31 (2009) 1225–1236.

21.Cui Weicheng, Huang Xiaoping, Wang Fang (2014), *Towards a Unified Fatigue Life Prediction Method for Marine Structures*, pp 215, Springer, 4 nov. 2014.

Received: April 12, 2022 / Accepted: June 15, 2022 / Paper available online: June 20, 2022